Annual and Nonseasonal Variability of Monthly Low-Level Wind Fields over the Southeastern Tropical Pacific

DAVID B. ENFIELD

School of Oceanography, Oregon State University, Corvallis 97331

(Manuscript received 4 March 1981, in final form 1 June 1981)

ABSTRACT

The time and space variability of low-level winds over the Southeast Tropical Pacific (SETP) region is described for the 6-year period 1974–80. The data set consists of monthly averaged low-level cloud-motion vector winds supplemented by coastal surface winds and pressure-related indices at fixed stations, and by long-term averages of ship-reported surface winds. The data are statistically analyzed in terms of correlations and empirical orthogonal functions (EOF's).

The annual cycle of the SETP low-level wind speeds is most prominent north of 15°S, with minimum and maximum intensities during the January–March and July–September periods, respectively, in phase with the larger scale southeast trades. South of 15°S the annual variability is small and characterized by minimum wind speeds from May through July, when the anticyclonic circulation center is at its northernmost position (~26°S). There is an SETP core region of maximum wind speeds that annually migrates (along 85°W) from 20°S in January–March to 15°S in June–August. Peru coastal winds are seasonally in phase with the southeast trade circulation at Talara (4°S) and San Juan (15°S) but considerably out of phase at Chimbote (9°S), Lima (12°S) and Tacna (17°S).

The nonseasonal component of the SETP circulation is characterized by areal coherence over the 15–30°S subregion. When the SETP circulation is unseasonally weak (strong), so is the intensity of the high-speed core, and both the core and the anticyclonic circulation center tend to lie north (south) of their climatological positions. A weak SETP circulation with northward lying positional characteristics prevailed during the 1976–77 El Niño. Nonseasonal variability is poorly correlated or uncorrelated between the coastal winds and various measures of either the basinwide or SETP circulations. Monthly anomalies of the low-level cloud-motion winds at 20°S, 85°W are an effective index of the nonseasonal atmospheric circulation of the SETP region.

1. Introduction

There has been an increased interest in the Pacific trade wind field due to recent work showing it to be a key feature of air-sea interaction phenomena that occur at interannual time scales (e.g., Wyrtki, 1975; Hickey, 1975; McCreary, 1976; Hurlburt *et al.*, 1976). Historically, analysis of the Pacific trades has been hampered by tropical ageostrophy and the scarcity of surface data. Wyrtki and Meyers (1976) developed an excellent set of bimonthly ship-reported Pacific wind data averaged over 2° latitude × 10° longitude quadrangles from 30°N to 30°S. Although they and others (Wyrtki, 1975; Hickey, 1975; Barnett, 1977; Goldenberg and O'Brien, 1981) have used this data set to improve our understanding of basinwide Pacific trade wind fluctuations, the details of the wind variability over the eastern South Pacific are still unclear, primarily because of the extreme scarcity of ship reports and lack of islands in that region.

Atlases (e.g., Hastenrath and Lamb, 1977) and Pacific trade wind studies (Wyrtki and Meyers, 1976; Barnett, 1977) suggest that wind intensity over the Southeast Tropical Pacific (SETP) is predominantly weakest during the Southern Hemisphere summer–fall season (February–March) and greatest during the winter–spring (August–September). But the nature of the annual north-south migration of the "core" region of greatest wind intensity, as well as that of the anticyclonic circulation center, remain unclear. Moreover, Goldenberg and O'Brien (1981) could not find an annual signal at 17°S from 84 to 104°W, while surface and sounding data at Lima suggest that in some places the coastal winds may be seasonally out of phase with the oceanic wind field of the SETP region (Enfield, 1981).

Wyrtki and Meyers (1976) and Barnett (1977) showed that the core region of the southeast trades as a whole varies interannually in both area and intensity, being weakest during El Niño episodes. This is particularly true in the central and western equatorial Pacific. However, Wyrtki and Meyers (1976) did not describe the interannual variability of the SETP region, and Barnett's (1977) eigenvector

0027-0644/81/102177-14$07.50

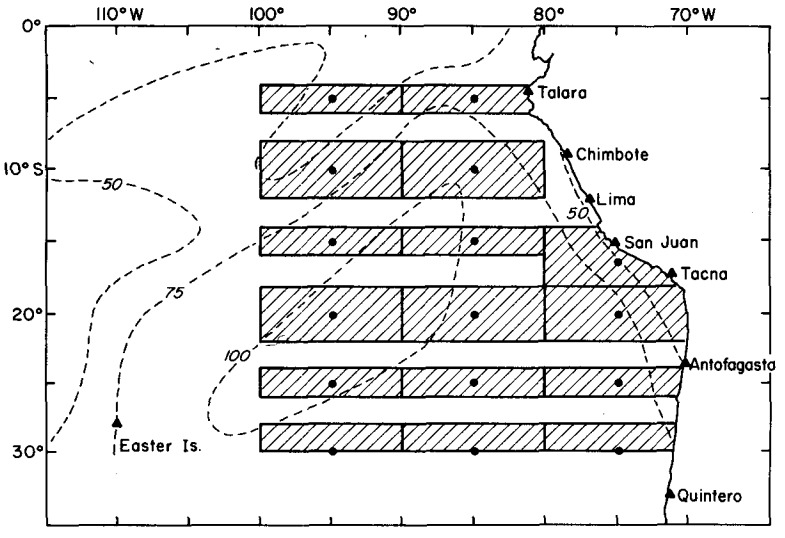

FIG. 1. Geographic distribution of monthly data used in the study. Solid circles: low-level cloud-motion vectors; triangles: surface wind speeds, sea level pressures and 850 mb heights; shaded areas: seasonally averaged surface wind vectors from ship reports; dashed curves: percentage of low-level wind observations provided by cloud-motion vectors for December 1972 (Ramage *et al.*, 1980).

analysis of the anomaly fields did not reveal a significant interannual signal there. Goldenberg and O'Brien (1981) found relatively high variability at periodicities of 20 months or more in the area between 15 and 25°S, 80 and 110°W, but did not specify the nature of those fluctuations. The charts of Kreuger and Winston (1975) show the 700 mb (3000 m) easterlies over the central and western equatorial Pacific to be anomalously weak or reversed during the 1972 El Niño, as were the surface easterlies, but stronger than normal over the SETP region. On the other hand, the monthly wind vector charts of Ramage *et al.* (1980) show the low-level winds in the SETP region to have been weaker during March–April, June and December 1972 (a strong El Niño) than during the same months of either 1971 or 1973. Similarly, Miller and Laurs (1975) found regional sea level pressure (SLP) differences to be relatively low in March, April, June, August, November and December 1972.

Wyrtki (1975) dispelled the previously held notion that the Peru coastal winds and upwelling weaken or cease during El Niño episodes, concluding that the ocean warming observed there during such episodes is remotely forced by a prior relaxation of the southeast trades over the central equatorial Pacific. Goldenberg and O'Brien (1981) also found interannual variability of ship reported winds to be low along the coast, while Enfield (1981) found the winds at the Lima airport to *increase* during El Niño episodes.

Clearly, previous studies have not focused on the winds of the SETP region because of the scarcity of data, and the subject is still fraught with contradictions and unanswered questions. This paper describes the annual and nonseasonal wind variability of the SETP region through an analysis of monthly averaged low-level winds compiled from satellite observations of cloud motion vectors from October 1974–September 1980. The density, representativeness and length of this data, together with surface and fixed-station observations, is sufficient to address a number of questions: 1) How are the annual and nonseasonal variabilities partitioned and distributed over the SETP region, including coastal South America? 2) What are the annual and nonseasonal meridional migrations of the high speed core and the anticyclonic circulation center? 3) What is the climatological shear field between the cloud level winds (~1–1.5 km high) and the surface? 4) How do the variabilities of the coastal and oceanic winds of the SETP region compare with each other and with that of the southeast trades as a whole? 5) To what extent can the nonseasonal variability of SETP winds be characterized by various indices of trade wind field behavior?

2. Data

Low-level winds are routinely inferred three times daily by NOAA's National Environmental Satellite Service (NESS) from low-cloud-motion vectors (CMV's) traced between successive infrared images from the Geostationary Operational Environmental Satellite (GEOS). These vectors are determined over a 2.5° latitude × 2.5° longitude staggered grid and are representative of the mesoscale patterns of convective clouds that move with the wind at levels

TABLE 1a. The 6-year (1974–80) average annual cycles and long-term means of the zonal (positive eastward) component of the low-level cloud-motion vectors at the points shown in Fig. 1.

Lat. (°S)	Long. (°W)	Month J	F	M	A	M	J	J	A	S	O	N	D	Year
5	95	−5.3	−5.3	−5.9	−5.4	−5.3	−6.0	−6.3	−6.4	−6.5	−5.3	−5.2	−5.0	−5.6
5	85	−4.6	−4.2	−4.4	−4.5	−3.7	−4.1	−3.8	−4.3	−4.0	−3.4	−3.0	−3.2	−3.9
10	95	−5.9	−5.6	−5.8	−6.2	−6.7	−7.2	−7.7	−8.1	−8.4	−6.9	−6.8	−6.3	−6.8
10	85	−4.0	−4.2	−4.1	−4.8	−5.0	−5.6	−6.4	−6.5	−6.9	−5.5	−5.0	−4.8	−5.2
15	95	−7.0	−7.6	−7.5	−7.4	−7.5	−7.4	−7.7	−8.7	−9.5	−7.7	−8.2	−7.3	−7.8
15	85	−5.2	−5.5	−5.6	−5.9	−6.9	−6.8	−7.4	−7.6	−8.0	−6.7	−6.6	−5.8	−6.5
16	75	−3.1	−3.9	−3.2	−4.3	−5.4	−5.5	−5.9	−6.4	−6.0	−5.3	−5.6	−4.1	−4.9
20	95	−7.0	−7.4	−7.8	−6.4	−5.6	−5.8	−5.4	−7.2	−8.2	−6.2	−6.6	−5.8	−6.6
20	85	−5.5	−6.1	−6.3	−5.6	−5.5	−5.9	−5.0	−6.4	−7.5	−6.1	−6.4	−5.6	−6.0
20	75	−2.9	−3.2	−4.1	−3.6	−4.1	−4.3	−4.2	−4.5	−4.7	−4.5	−4.1	−3.6	−4.0
25	95	−4.8	−5.1	−5.3	−3.4	0.1	−0.7	0.4	−2.4	−3.9	−2.0	−3.1	−3.5	−2.8
25	85	−4.5	−4.2	−4.7	−3.0	−1.5	−0.9	−0.6	−2.1	−3.6	−2.4	−3.4	−3.9	−2.9
25	75	−2.2	−1.6	−2.4	−1.3	−1.4	−1.0	−0.5	−0.8	−1.6	−1.9	−2.0	−2.3	−1.6
30	95	−0.2	−0.5	0.0	1.0	6.0	4.4	5.9	3.5	1.3	3.9	2.4	1.8	2.5
30	85	−0.4	−0.0	−0.6	−0.4	4.9	2.9	3.8	2.5	1.0	1.9	1.8	0.2	1.5
30	75	−0.7	0.8	−0.4	0.6	2.6	2.2	2.9	1.8	1.9	0.9	0.8	−0.5	1.1

usually between 1000 m (900 mb) and 1500 m (850 mb). Typically, 3000–4000 CMV's are obtained each day for the tropical Pacific as compared with only 50 wind observations from ships. Cloud-motion winds provided more than 75% of the data in the SETP region used by Ramage *et al.* (1980) to document the 1971–73 El Niño cycle (Fig. 1).

Since October 1974 the University of Hawaii has produced tropical Pacific streamline analyses from monthly averaged cloud motion data. The monthly streamline analyses for the SETP region were generously provided by J. Sadler for the 6-year period from October 1974–September 1980. On each analysis, two CMV vectors separated by 2.5° latitude spanned each of the 16 solid circles shown in Fig. 1. Each pair of vectors was read off and averaged to give the monthly speed and direction at each point. Analyses were missing for November 1974 and April, June and August 1975. These gaps were filled by linear interpolation.

Monthly averaged surface wind speeds were obtained for five Peruvian coastal airports: Talara (4½°S), Chimbote (9°S), Lima-Callao (12°S), San Juan (15°S) and Tacna (17°S), shown in Fig. 1. These data are scalar averages of wind speeds read from anemometers at 3 h intervals. Because of the steadiness of the coastal winds (Enfield, 1981) the data may be treated as vector speeds, directed equatorward and alongshore, but with a small onshore component.

To investigate pressure indices for the SETP circulation, monthly averaged sea level pressures (SLP) were obtained from the same airports plus Easter Island and Darwin, Australia. To see if

TABLE 1b. As in Table 1a except for the meridional (northward) component.

Lat. (°S)	Long. (°W)	Month J	F	M	A	M	J	J	A	S	O	N	D	Year
5	95	1.6	1.9	1.4	1.9	3.3	4.4	4.7	5.1	5.3	4.9	4.2	3.7	3.5
5	85	2.1	1.4	1.5	2.5	4.0	4.4	5.2	6.1	6.0	5.3	4.8	3.9	3.9
10	95	3.2	2.4	2.5	2.7	3.2	3.6	4.5	4.7	5.0	4.5	3.8	3.4	3.6
10	85	2.8	2.7	2.7	3.4	4.3	4.9	5.4	5.9	5.9	4.9	4.6	3.9	4.3
15	95	3.0	2.8	2.5	1.9	2.1	2.7	3.3	3.7	3.7	3.6	3.5	3.0	3.0
15	85	3.6	2.9	3.4	3.4	4.1	4.5	5.3	5.9	6.5	5.2	4.9	3.8	4.5
16	75	3.0	2.7	2.9	4.2	4.9	5.5	6.4	6.5	6.8	5.7	5.3	3.9	4.8
20	95	3.6	3.4	3.0	1.8	1.1	2.0	2.9	2.6	3.4	2.8	3.2	3.6	2.8
20	85	4.6	4.5	4.3	3.9	4.4	4.6	5.1	5.6	6.4	5.0	5.2	4.4	4.8
20	75	4.5	4.6	4.3	5.0	6.1	6.2	6.7	7.2	8.0	6.5	6.0	5.1	5.8
25	95	2.6	2.9	2.3	1.5	0.7	2.3	3.5	2.7	2.7	2.7	2.7	2.3	2.4
25	85	5.2	5.3	5.1	4.5	4.4	4.3	5.0	5.8	6.5	5.3	5.3	4.6	5.1
25	75	6.5	6.5	6.7	4.3	6.7	4.7	7.1	7.2	8.6	7.6	7.3	7.0	6.7
30	95	2.1	3.0	2.5	1.1	2.6	3.5	4.3	3.1	3.1	3.0	3.0	2.3	2.8
30	85	5.2	5.0	4.8	2.9	4.3	4.3	5.4	3.3	6.6	5.0	5.3	4.6	4.7
30	75	7.3	6.8	7.1	6.2	6.1	5.5	5.7	2.9	7.6	7.1	6.7	7.3	6.3

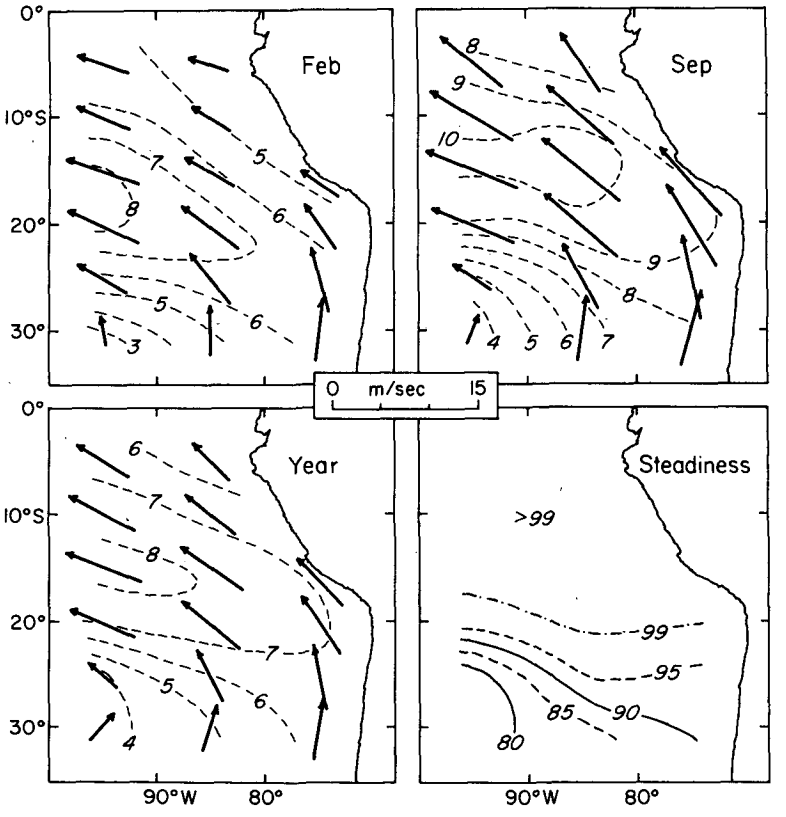

FIG. 2. First three panels: Maps of 6-year mean vectors (arrows) and isotachs (dashed curves) for climatically antipodal months and the whole year, from low-level cloud-motion vectors. Fourth panel: distribution of directional steadiness of monthly cloud-motion vectors (percent).

pressure variations near the cloud level were more representative than SLP, monthly averaged 850 mb heights were obtained for Easter Island, Lima, Antofagasta and Quintero (Fig. 1).

For evaluation of the shear fields between the surface and the cloud level, G. Meyers kindly provided the long-term means of the 1900–73 ship-reported winds for 2° latitude × 10° longitude quadrangles in the SETP region and for each month of the year. This is a geographic subset of the data analyzed by Wyrtki and Meyers (1976). Where a quadrangle contains one of the 16 chosen CMV points, the original zonal and meridional component averages were accepted as such. Where a CMV point fell between two quadrangles, the means were averaged into a 4° × 10° quadrangle. Quadrangle data did not exist south of 30°. The areas covered by the final set of averages are shaded in Fig. 1.

3. Annual variability

a. Cloud-motion winds

The 6-year average annual cycle and long-term mean for the CMV winds were computed vectorially for each of the 16 points shown in Fig. 1. The zonal and meridional components of these averages are listed in Table 1. Areawide, the seasons of weakest and strongest winds are centered near February and September, respectively. The vector/isotach maps for these months and for the annual

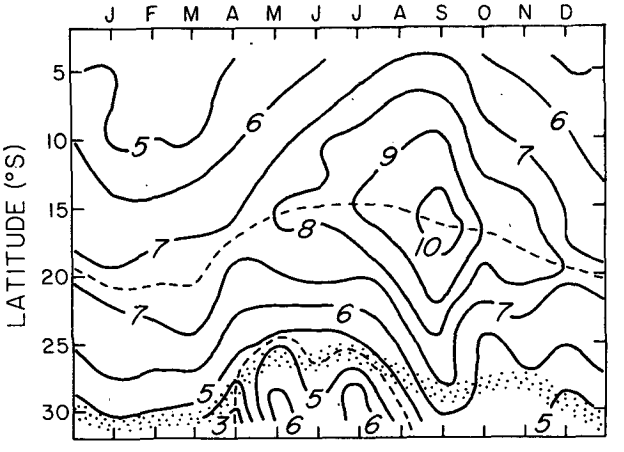

FIG. 3. Annual variation of 6-year vector mean wind speed along 85°W longitude, from low-level cloud-motion vectors. Minimum and maximum are traced by dashed curves. Stippled shading indicates the scalar averaged speed minimum, representative of the meridional movement of the anticyclonic circulation center.

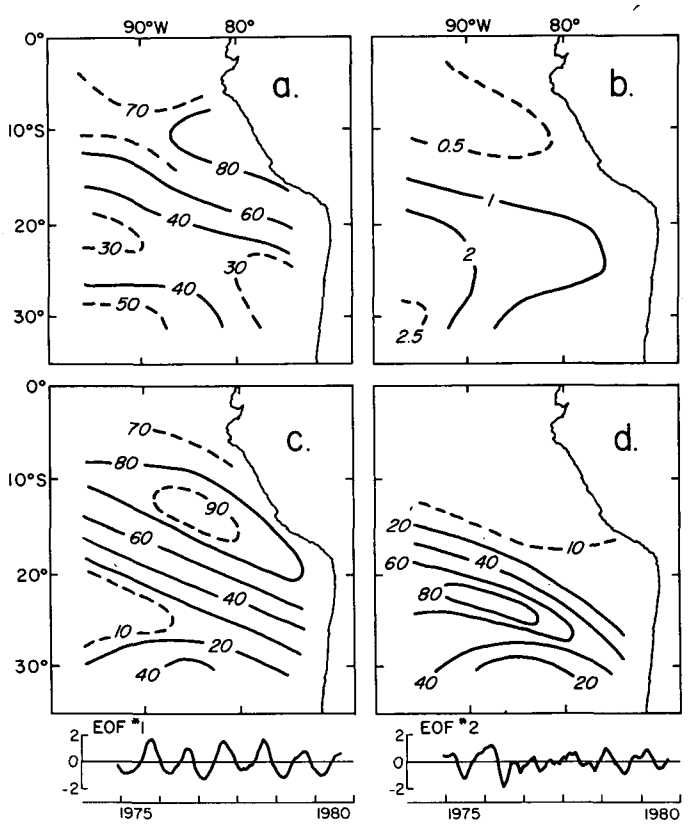

FIG. 4. Distribution of low-level cloud-motion vector variability: (a) annual variability expressed as a percentage of total variance ("seasonality"); (b) residual variance (m^2 s^{-2}) after subtraction of 6-year mean annual cycle; (c) percentage of total variance explained by the first EOF of the unaveraged monthly data; (d) same, for second EOF. Bottom: amplitude time series (standard deviation units) corresponding to EOF distributions of (c) and (d).

mean field are shown in Fig. 2. The distribution of directional steadiness between months (the vector mean speed divided by the scalar mean speed and expressed in percent) is also shown.

The strongest winds tend to occur in a core region that extends from 15°S, 95°W to 20°S, 75°W. The weakest and most directionally unsteady winds are found in the southwest corner of the area, due to the proximity and movement of the anticyclonic circulation center of the SETP region.

Within the core (regardless of its position) the speeds change by ~3 m s^{-1} over the year, and directional changes are small. The wind direction veers (clockwise turning) systematically in the north from summer (February–April) to winter (August–October). As a consequence of this veering, combined with the meridional shift of the core, the vector difference between the two seasons (not shown) has its greatest magnitude in the northeast corner of the SETP region (>4 m s^{-1}).

A time-latitude contour plot of the vector mean speed along 85°W more clearly illustrates the meridional movement and/or intensity changes of the principal circulation features during a typical year (Fig. 3). The core of maximum vector mean speed moves meridionally from 21°S during January–March, with values of 7–8 m s^{-1} to 15–16°S during May–August, with a yearly peak of ~10.5 m s^{-1} in September. This behavior also characterizes the scalar-averaged values because of the large directional steadiness in that latitude range (Fig. 2). A minimum of vector mean speed migrates northward into the southern portion of the study area (25–30°S) from April–August, parallel to the behavior of the high-speed core further north. The corresponding scalar average of minimum speeds (stippled) undergoes a similar but less pronounced north-south migration, the difference being due to the greater directional variability of this area. Because the scalar-averaged minimum follows the true meridional movement of the feature, it is the more meaningful of the two.[1]

[1] It should be noted that the latitudinal positions of the circulation features, discussed throughout this paper, were determined directly from the original streamline analyses, on which CMV vectors were plotted at 2.5° intervals. Hence, their positional resolution is better than that implied by Fig. 1.

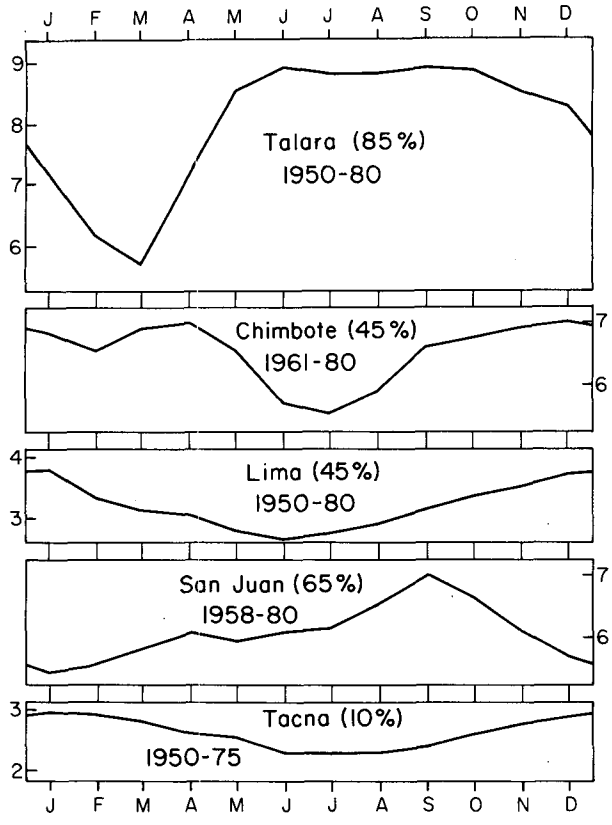

FIG. 5. Mean annual variations of monthly wind speeds (m s^{-1}) at Peruvian airports, 1950–80. Percentages in parentheses are seasonalities as defined in the text.

The scalar speed minimum (stippled) coincides with the latitude where the wind trajectory backs from southwesterly through southerly to southeasterly. It marks the eastward extension of the anticyclonic circulation center and, by inference from geostrophy, corresponds to the South Pacific high-pressure ridge. The meridional position of this feature undergoes a 5° latitude migration northward from 31°S in summer (January–March) to 26°S in fall–winter (May–July).

The latitudinal displacements of the anticyclonic circulation center itself follow closely those of the scalar speed minimum, with a mean meridional location near 25–30°S. The center usually lies west of the study area and undergoes large zonal excursions from month to month. From October–January it tends to lie farther westward (100–140°W) than during the remaining eight months (90–120°W). Note, for future reference, that Easter Island (Fig. 1) lies near the climatological center of the ellipsoid described by the positional variability of this feature.

The variance distribution of the annual and nonseasonal components of wind speed over the SETP region is characterized by two methods (Fig. 4): direct separation of the components by averaging, and separation through empirical orthogonal function (EOF) analysis. Both analyses were scalar computations. At each point the mean annual cycle was computed and subtracted from the data and the residual (nonseasonal) variance determined. The annual variance was then found by subtraction of the residual variance from the total. The annual variance, expressed as a percentage of the total variance, is herein defined as the seasonality (Fig. 4a). It is maximum in the northeastern part of the region, offshore of the north-central Peru coast; the lowest seasonality extends along a quasi-zonal band from 20°S, 95°W to 25–30°S, 75°W. The respective annual cycles are typified by the latitude ranges 10–15°S and 20–25°S in Fig. 3. The nonseasonal (residual) variance is greatest in the southwestern part of the region (Fig. 4b).

The first two modes of the EOF analysis of wind speed account for 46 and 31% of the total variance and model the subregions of strongest and weakest seasonality, respectively. The geographical distribution of the variance explained by these modes is shown in Figs. 4c and 4d. The seasonality of the time coefficients is 82% for EOF#1 and 47% for EOF#2, and their annual cycles (Fig. 6) are also similar to those at corresponding latitudes in Fig. 3. Note that a considerable phase lag exists between the sectors represented by these modes. This lack of contemporaneous annual coherence explains why more than one mode is needed to extract the annual variability of the region. Barnett's (1977) analysis of the Pacific trades as a whole gave similar results.

The two analysis methods represented in Fig. 4 provide a consistent picture of the distribution of annual variability over the SETP region. Interannual variability is also apparent in the two EOF time series, e.g., the Southern Hemisphere winters of both 1976 (a moderate El Niño) and 1979 had anomalously weak circulations. More efficient indicators of such variability are discussed in a later section.

b. Coastal winds

The annual cycles and seasonalities of the wind speeds at five coastal airports are shown in Fig. 5 (see Fig. 1 for locations). Talara and San Juan have the largest seasonalities and more closely resemble the seasonal cycles of the offshore cloud level winds, with minima and maxima in the summer and winter seasons, respectively. At the other locations the annual variability is considerably phase-shifted from that of the offshore winds and accounts for less of the total variance.

From an analysis of the Lima winds, Enfield (1981) explained this dichotomy in terms of insolation differences from one part of the coast to another. Chimbote, Lima and Tacna are typified by persistent

stratiform winter cloud cover, several hundred meters high and just below the regional inversion, which prevents differential heating of the desert air with respect to the air over the nearshore sea surface. Conversely, the relative lack of summer clouds at these locations induces desert heating and a higher sea-to-land pressure gradient. Thus, summer wind speeds tend to be enhanced and winter ones suppressed, contrary to the offshore circulation. This seasonal contrast of alongshore geostrophic effects is less pronounced at Talara and San Juan because stratiform clouds are dissipated over the larger desert areas of those locations, which remain relatively sunny year-round.

c. *Pressure indices*

It is natural to look for indices of the wind behavior that can be used as monitoring tools, in view of the scarcity of data. The Southern Oscillation Index (SOI), or sea level pressure (SLP) difference between Easter Island and Darwin, Australia, has often been used as a measure of Pacific trade wind variability on interannual time scales, and correlates well with the oceanic anomalies of El Niño episodes (e.g., Quinn, 1974; Enfield and Allen, 1980). Miller and Laurs (1975) used regional SLP difference as an indicator of anomalous wind behavior over the SETP region during the 1972 El Niño.

One index examined in this study was the SOI, since it presumably characterizes the behavior of the Pacific SE trade wind system as a whole, of which the SETP region may fluctuate as an integral part. But it also seems appropriate to try the approach of Miller and Laurs (1975), i.e., to characterize the pressure gradient across the SETP region. For the high-pressure end of their SLP differences, they read or interpolated pressures off of 12 h National Meteorological Center (NMC) surface charts, at 30°S, 90°W, and block-averaged to weekly values. This is no longer feasible, as NMC has stopped analyzing pressure over this region; in any case, the method always involves uncertainty due to the scarcity of surface ocean data there. Because the displacements of the anticyclonic circulation center (determined independently from CMV analyses) tend to occupy the area between 25–30°S and 90–140°W, Easter Island seems especially appropriate as the high pressure end of a regional SLP index. The low-pressure end was taken to be Lima because upper air data are also available from both Easter Island and Lima. Hence, the heights of the 850 mb pressure surface (close to the level of CMV traces) could be examined, as well as SLP. As a check, Easter Island was also differenced with other Peru coastal stations (SLP) and with Antofagasta and Quintero (850 mb height).

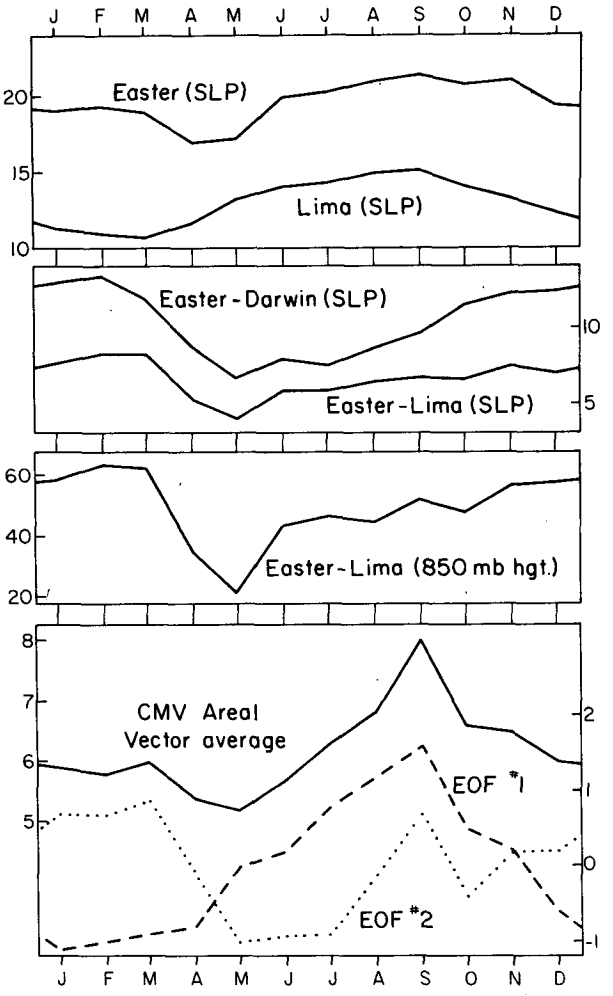

FIG. 6. Mean annual variations of 1950–80 Easter Island and Lima sea level pressure (mb); 1950–80 Easter minus Darwin (SOI) and Easter minus Lima SLP differences (mb); 1970–80 Easter minus Lima 850 mb height difference (m); cloud-motion wind speed (m), vectorially averaged over the region, and the two EOF time series of Fig. 4 (standard deviation units).

The annual cycles of some of the pressure difference indices, plus the Easter Island and Lima SLP components, are shown in Fig. 6. For comparison, annual cycles also are shown for several measures of the regional (CMV) wind variability: the two EOF modes already discussed and the magnitude of the wind, vectorially averaged over the region. Clearly, the EOF modes represent subregions of variability that act as components of the regionally averaged wind, with its peculiar minimum centered in May. The overall wind variability seems best represented by SLP at Easter Island, rather than by any of the pressure or height differences. The annual cycle of the SOI is dominated by the pronounced winter minimum of SLP at Darwin (not shown), while Lima SLP is probably greatly influenced by the continental low and land-sea ef-

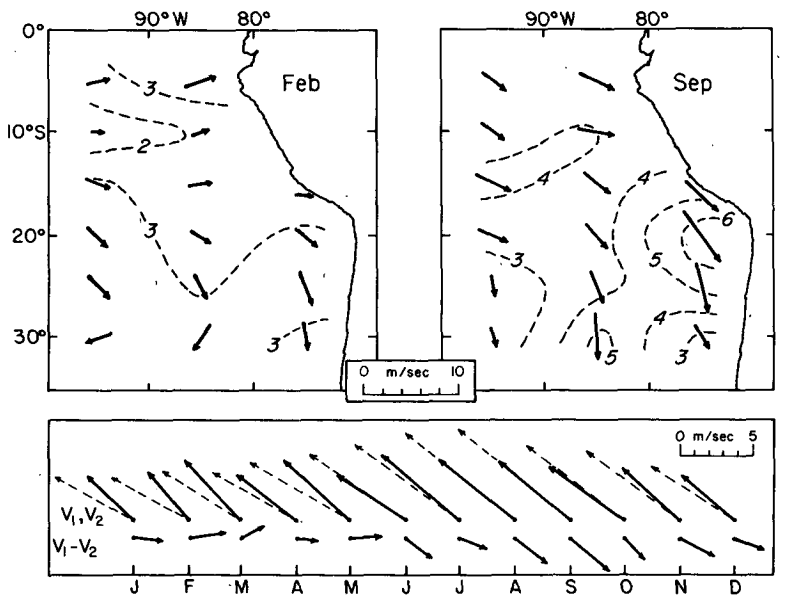

FIG. 7. Top: maps of vectors (arrows) and isotachs for the vertical shear between the long-term means of the Wyrtki-Meyers surface winds (1900–73) and the low-level cloud-motion vectors (1974–80). Bottom: annual variation (at 15°S, 85°W) of long-term mean vectors of surface wind (V_1, solid), cloud-motion wind (V_2, dashed) and their difference ($V_1 - V_2$).

fects and therefore acts more as a component of the coastal rather than the large-scale pressure system. The 850 mb height difference, dominated by the Easter Island component (the Lima component is virtually constant), reflects the minimum winds in May, but not the September maximum. Pressure and height differences between Easter Island and the other South American coastal stations give essentially the same results as shown in Fig. 6 for Easter Island and Lima.

4. Shear climatology

How representative are the cloud-level winds of the surface winds that can influence upper ocean characteristics? Basically, that representativeness can be diminished by several factors: 1) the natural variability in the boundary-layer profile between the two levels (due at least in part to changes in atmospheric stability); 2) the wind shear "contamination" of CMV estimates due to the natural variability in convective cloud heights; and 3) the uncertainties inherent in the estimation procedure itself. All of these are considerably influenced by the unpredictability or random nature of convective motions at subsynoptic time and space scales. Hence, one would anticipate more representativeness at lower frequencies for which time averaging can be expected to smooth out the randomness. This is confirmed by several studies. For example, day-to-day wind profiles from soundings in the tropical boundary layer vary randomly about their monthly means, but the monthly averaged profiles tend to remain stable about longer time scale means (Mendenhall, 1967; Gray, 1972). Another study by Halpern and Knox (1981) found high spectral coherence between the easterly components of buoy winds and the NESS CMV winds, near 152°W on the equator and at frequencies below 0.17 cycles per day (cpd). Monthly averages of the two have a correlation of 0.88 for the 9-month period from May 1979–January 1980. Hence, the indications are that the CMV winds over the tropical Pacific can be successfully used to infer surface winds on time scales resolvable with monthly averaged data.

Sadler (private communication) has derived the monthly mean Pacific surface trades by applying a climatological mean shear field to individual monthly analyses of cloud-level (CMV) winds. The procedure for extracting the shear field involves subtracting the 5-year mean (1975–79) field of satellite winds for each month of the year from the corresponding long term mean (1900–73) surface field based on ship winds. The divergence field from his surface analysis for November 1979 compared favorably with the vertical motion field inferred from the highly reflective cloud distribution over the tropical Pacific for the same month. This is considered a severe test of wind field accuracy.

The 1900–73 mean zonal and meridional components of ship-reported surface winds were obtained and recomputed for the quadrangles shown in

Fig. 1. The corresponding 1974–80 means from Table 1 were then subtracted to form the shear components between the surface and low-cloud level. The preferable procedure (had it been feasible) would be to use the mean surface fields for the same period (1974–80). However, there were an average of only three ship reports per month per 10° square in a critical region (15–30°S, 80–100°W) during the period. The statistical uncertainties of taking averages of such data make it preferable to use the larger (1900–73) surface data base, in spite of the possible nonstationarity between the different averaging periods.

The vector/isotach shear fields are shown in Fig. 7 for February (summer) and September (winter), along with the annual variation of the surface, cloud level and shear vectors at 15°S, 85°W. The two shear fields may be compared with the corresponding CMV fields shown in Fig. 2.

Overall, the long-term mean and seasonal variability are quite similar for the surface and low-cloud wind fields. As one would anticipate for frictional effects in the Southern Hemisphere, the surface wind predominantly veers from the cloud level wind and is weaker. The veering tends to be small (0–20°) over much of the region and year but greater close to the equator where geostrophy is weak. Also, differences in speed between the two levels are larger during winter months, whereas the amount of directional veering is greater during the summer months. The fact that the mean shear field characteristics are consistent with the expected behavior of the planetary boundary layer tends to confirm the validity of Sadler's shear-subtraction procedure as a means of obtaining representative (monthly) surface wind fields from cloud-motion data.

In the following section, the annual cycles (Table 1) are subtracted from the CMV wind data to obtain residual (anomaly) time series. Strictly speaking, such residual time series represent the anomalous wind variability only near the cloud level. However, to the extent that it is valid to apply a climatological wind shear to the CMV data to obtain surface winds, the CMV residuals are also representative of surface wind anomalies. This is because the shear-correction procedure only alters the mean wind for each time series and each month of the year, such that subsequent subtraction of the annual cycle yields the same residuals as if no correction had been made. This is significant for oceanographers, as it implies that the results of Sections 6 and 7 regarding the anomalous cloud-level wind are also applicable (at least qualitatively) to the surface wind behavior as well. It also provides a rationale for blending monthly surface and cloud-level data to study nonseasonal low-level wind variability.

A few words of caution are in order for those who would interpret cloud-motion vectors in terms of surface winds. Even under the assumption that the non-seasonal shear variability is small, the climatological shear itself has spatial and seasonal variations (e.g., Fig. 7) that would generally invalidate the surface applicability of mean annual and seasonal cloud-level wind distributions. In addition, it cannot be assumed that monthly departures from seasonal mean shears will be small everywhere (this study and most of those cited above apply only to specific locations or areas). In particular, it appears that this assumption may be untenable for the region between Ecuador and the Galapagos Islands (Sadler, personal communication).

5. Nonseasonal variability

The nonseasonal variability of the variables discussed in this paper is represented in the residual (anomaly) time series after the mean annual cycles have been removed. This variability contains both interannual and within-year (<12 months) time scales, which cannot be separately examined through spectral decomposition techniques because of the short record lengths involved. However, the interannual time scale typically accounts for most of the variance, a fact that should be kept in mind even though the term "nonseasonal" is conservatively applied except where interannual features are specifically discussed.

The scalar-averaged annual cycles of the CMV wind speeds (Section 3) were subtracted from the original monthly (vector) speeds at each of the 16 points of the SETP grid (Fig. 1) to yield the corresponding residual time series. With the assumption that the monthly nonseasonal shear variability is small (Section 4), the residual series for surface wind speeds at the five Peruvian airports (Fig. 1) can rationally be blended with the CMV residuals to obtain more complete field representations over the SETP region.

Two univariate time series were computed as measures of the regional nonseasonal variability of the SETP circulation strength. The first, termed the *average speed anomaly*, is simply the scalar average of the speed residuals over the CMV grid (the 16 points in Fig. 1). The second, termed the *anomaly mode*, is the first eigenvector time series for the complete anomaly field (the 16 CMV points plus the five Peruvian airports). To further characterize the nonseasonal circulation, three diagnostic descriptor variables were determined from the CMV streamline analyses along 85°W, and their residuals were computed. They are the wind-speed magnitude of the high-speed core; the latitude of the high-speed core; and the latitude of the speed minimum that extends eastward from the anticyclonic circulation center. The annual variability of these features was discussed in Section 3.[1]

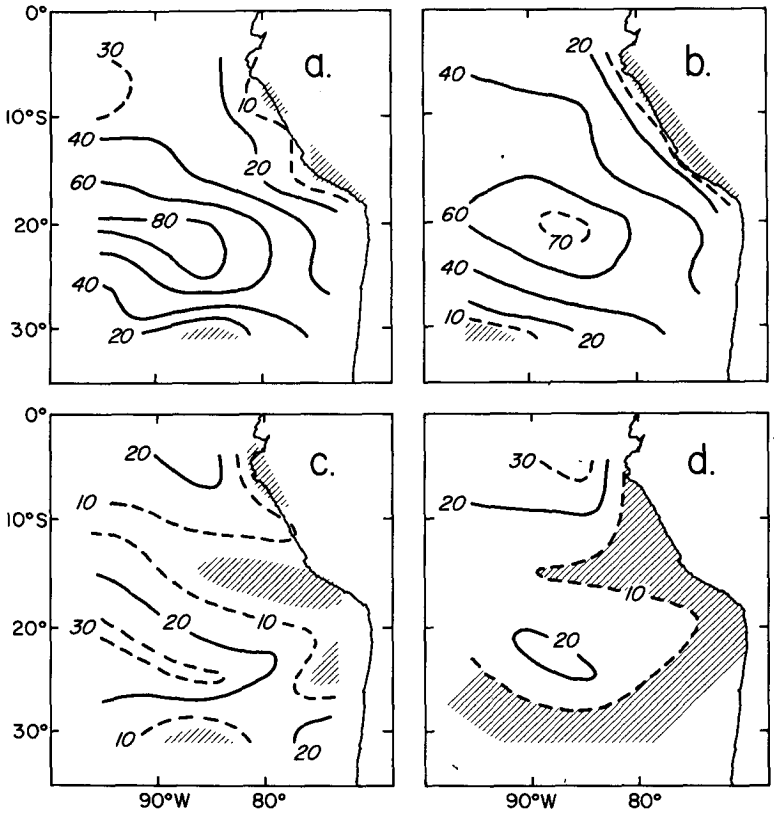

FIG. 8. Distributions of specification skills (%) (defined in the text) between residuals of the combined cloud-motion and coastal winds and: (a) their first EOF (the anomaly mode); (b) the average speed anomaly of the cloud-motion winds; (c) the Easter Island sea level pressure anomaly; and (d) the SE trade area index anomaly. Shading indicates significance at <95% statistical confidence.

Residual time series were also examined for a number of proxy variables. Potential indices for SETP wind behavior include the surface pressure (SLP) and 850 mb height at Easter Island as well as their differences between Easter Island and Lima. To represent the Pacific-wide behavior of the SE trades, two indices were used: the SLP difference between Easter Island and Darwin, Australia (SOI), and southeast trade area index (Sadler and Kilonsky, 1981). The SE trade area index is defined as the area east of 180°W covered by CMV wind speeds (south of the intertropical convergence zone) in excess of 8 m s^{-1} and having a predominant easterly component. Such core areas have been shown to be representative of southeast trade wind fluctuations by Wyrtki and Meyers (1976) and Barnett (1977).

The variable that explains the greatest amount of nonseasonal speed variance over the SETP region is the anomaly mode (45%). The next three eigenvectors individually account for much less overall variance (15, 11 and 8%) and represent, respectively, the localized variability (1) near the South Pacific high pressure ridge, 25–30°S; (2) in a swath extending from northern Chile and southern Peru westward to 10°S, 95°W; and (3) the north-central Peru coast.

The correlation of the anomaly mode with other variables is summarized in Table 2. In addition to the raw maximum-lagged cross correlation (r), the large-lag standard error of the cross correlations (σ) was used to compute normalized correlations ($|r|/\sigma$) and effective specification skills (S). Under the assumption of bivariate normality, normalized correlations of 1.8, 2.0, 2.6 and 3.3 correspond to significance levels at 90, 95, 99 and 99.9% confidence, respectively (Sciremammano, 1979). The specification skill is defined as the percentage of variance explained in one variable by the other after correction for the correlation due to random associations, i.e., $S = 100(r^2 - \sigma^2)$.

The SETP regional wind variability, as represented by the anomaly mode, is correlated with all variables at the 99% significance level or better. It is highly representative of the average speed anomaly (S = 77%). As the overall SETP circulation (anomaly mode) increases, the anticyclonic

ridge (Easter SLP) and the high-speed core intensify, and their extensions near 85°W tend to be found south of their normal positions. These events are contemporaneous with an increase in the Southern Oscillation Index and precede a geographic expansion of the basinwide southeast trade wind field by a month. Because the SOI and the SE trade area index decrease in association with El Niño episodes (Quinn, 1974; Wyrtki and Meyers, 1976), their positive correlations with the anomaly mode imply an overall weakening of the SETP circulation in conjunction with those events; similarly, the correlations of the positional features with the anomaly mode imply that they are north of their normal latitudes during El Niños. Finally, a good proxy index for nonseasonal SETP circulation changes is the anomaly of surface pressure at Easter Island.

The distributions of the nonseasonal wind variability explained by the anomaly mode, average speed anomaly, and residuals of the Easter Island SLP and southeast trade index are shown in Fig. 8. These were determined from maximum-lagged cross correlations (lags not shown). The similarity of the first two panels (Figs. 8a and b) verifies the overall representativeness of the anomaly mode. Note that the nonseasonal wind speeds are best specified by the first three variables (Figs. 8a–8c) over the area west of 75°W and somewhat south of the high-speed core (see Fig. 3). The near-equatorial sector is the one best specified by the southeast trade index and leads the latter by 3–4 months (Fig. 8d); the larger area of lower skill to the south leads the southeast trade index by 0–1 months. All other significant correlations (Figs. 8a–8c) were strongest at zero lag.

The winds in the coastal sector are only marginally coherent with the offshore circulation (Figs. 8a and 8b) and unrelated to large-scale circulation indices (Figs. 8c and 8d). The wind speed at Lima has a correlation of −0.33 with the areally averaged CMV speeds and leads them by five months. Hence, there is a tendency for the Lima winds to strengthen when the offshore circulation is weaker, such as during El Niño episodes. Except for Chimbote (0.26, 5-month lead) the corresponding correlations for the other coastal stations were insignificant at the 95% confidence level. These results are consistent with the analyses of Wyrtki (1975) and Enfield (1981).

6. Interannual changes

The time series plots of the anomaly mode, southeast trade area index and Easter Island SLP residuals illustrate the interannual variability during the 1974–80 period (Fig. 9). Other variables, such as the Southern Oscillation Index (Quinn, 1974) and the areal average of CMV speeds, show a similar

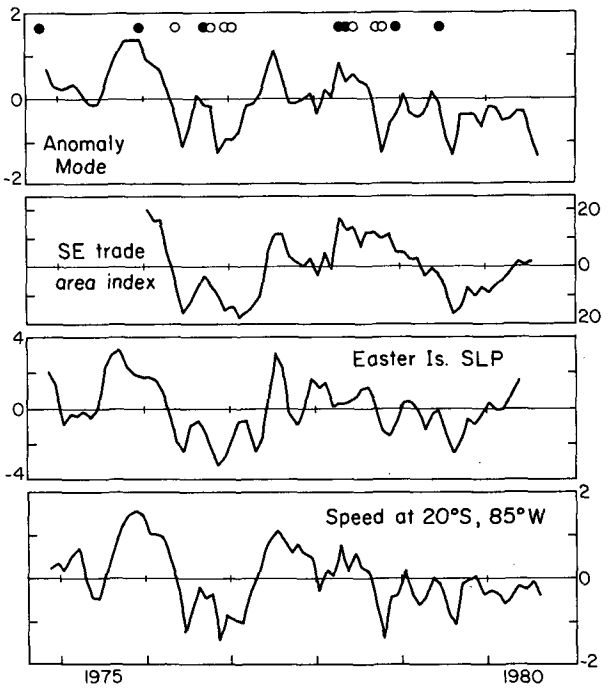

FIG. 9. Three-month running mean time series of the anomaly mode (standard deviation units); the SE trade area index anomalies (2×10^5 km^2); Easter Island SLP anomalies (mb); and the cloud-motion speed anomalies at 20°S, 85°W (m s^{-1}). Open (solid) circles at the top of the figure indicate months when both speed extrema were 2° latitude or more north (south) of normal.

behavior. The circulation in the latter half of 1975 and the first few months of 1976 was stronger than normal, then became anomalously weak until mid-1977. The weak circulation of 1976–77 coincided with a moderate El Niño episode (Wyrtki, 1979). The circulation strength then increased over the next 15 months and again weakened from the end of 1978 until the beginning of 1980.

The nature of the circulation anomalies associated with the 1975–77 El Niño cycle can be seen in the three-monthly vector residual fields from October 1975–July 1977 (Fig. 10). During the pre-El Niño phase (October 1975, January 1976) the winds along 20–25°S had a stronger easterly component than normal; north of there the winds were somewhat more southerly than normal. In April 1976 (a transitional month) the easterly anomalies persisted but shifted further south, and northerly anomalies began to appear off northern Peru. The El Niño phase (July and October 1976; January 1977) was characterized by strong westerly anomalies and weak northerly anomalies over most of the SETP region. April 1977 was again transitional, then strong southeasterly anomalies returned in July 1977.

The anomalies during the El Niño phase (July 1976–January 1977) were generally not large enough

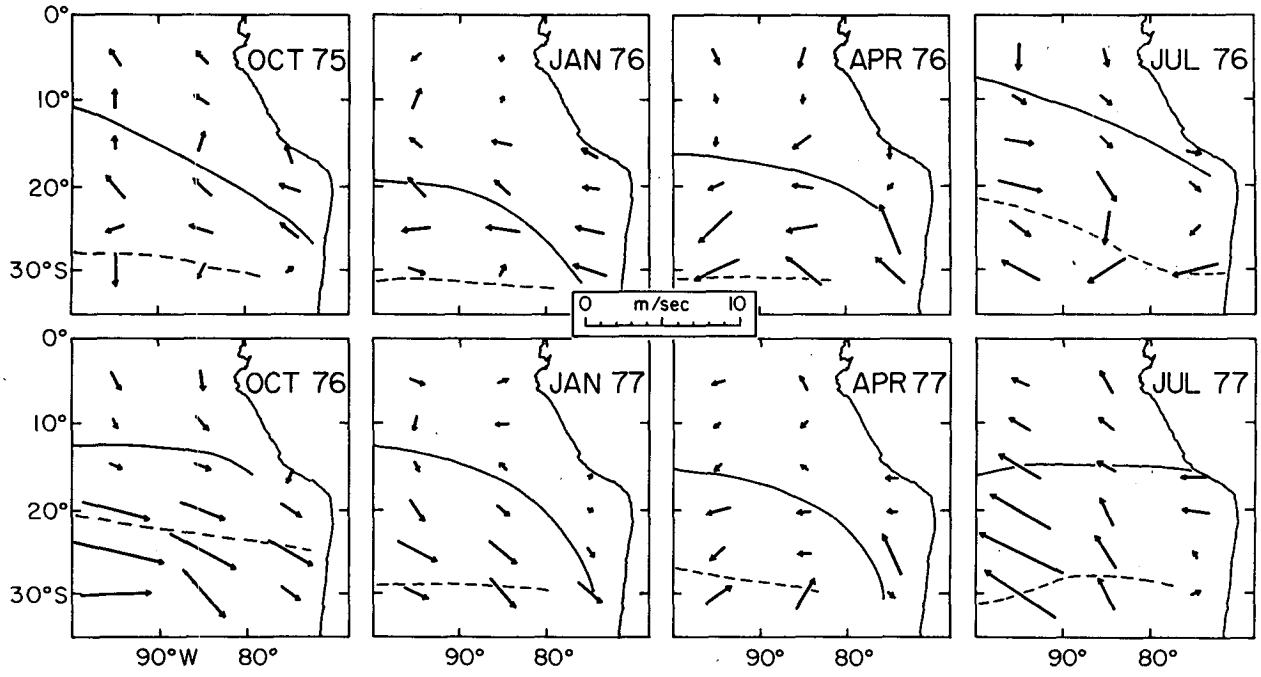

FIG. 10. Cloud-motion vector anomaly maps for every third month during the 1975–77 El Niño cycle. Solid (dashed) curve is the axis of the maximum (minimum) speeds for each month.

to constitute a flow reversal, rather, significant weakening from mean seasonal values (Figs. 2 and 3). The subregion most affected was 20–30°S, 80–100°W, with wind strength reductions of 30–50% in July 1976 and January 1977, and 40–80% in October 1976. This behavior is also representative of months not shown in Fig. 10 with one exception: the circulation strengthened briefly in September 1976, with speeds ~30% above normal in the above subregion. The pattern of weakened winds during the 1976–77 El Niño is confirmed by the anomaly mode plot (Fig. 9), but there the September 1976 reversal of anomalies is attenuated while the anomalies of August and October appear small (this is due to the smoothing effect of the 3-month running mean filter used for the plots in Fig. 9).

The combined Peru coastal wind speeds during the 11-month El Niño period from May 1976 through March 1977 averaged an insignificant 3% above the 30-year mean value, with a standard deviation of 13%. Only the Lima speeds departed from their long-term mean by more than 10% (17 ± 14% greater). The latter feature is consistent with Enfield's (1981) analysis for wind soundings at Lima.

The axes of the high- and low-speed extrema are also shown in Fig. 10. Note that these features do not generally coincide with extrema of the anomaly vectors, and that they undergo similar meridional displacements. Over the 6-year period (1974–80) the anomalous displacements of the two-speed extrema were positively correlated with each other ($r = 0.66$), but their standard deviations were only ~2° of latitude. Hence most of the non-seasonal displacements are smaller than the effective resolution of the data. On 14 occasions both features were displaced by 2° of latitude or more from their normal positions and in the same sense (Fig. 9). The departures from normal for the 14 events averaged about 4° of latitude, with a maximum of 8°. Therefore, these anomalous displacements were at least comparable to the mean seasonal displacements (Fig. 3) and were reasonably well resolved by the CMV streamline analyses.[1] Five of these events occurred during the 2-year period of Fig. 10—all of them within the El Niño phase. Of these, four events were anomalous northward displacements of 3–4° (May, October, December 1976; January 1977) and one was southward

TABLE 2. Statistics for variables that were lag correlated against the anomaly mode. The symbols r, σ are the maximum lagged correlation and the large-lag standard error, respectively; $S = 100\,(r^2 - \sigma^2)$.

Variable	Std. dev.	r	$\lvert r\rvert/\sigma$	S	Lag
Average speed anomaly	0.64 m s^{-1}	0.89	6.6	77	0
Speed core intensity	0.73 m s^{-1}	0.80	5.9	62	0
Speed core latitude	1.92° lat	0.40	3.4	15	0
Speed min. latitude	2.11° lat	0.62	5.1	37	0
Easter Island SLP	2.29 mb	0.63	4.6	38	0
Easter 850 mb hgt.	1.87 m	0.58	4.3	32	0
Easter-Lima ΔH_{850}	1.71 m	0.63	4.3	38	0
Southern Oscillation	2.68 mb	0.61	4.4	35	0
SE trade area index	2 × 10^6 km^2	0.44	2.7	17	1

(September 1976). The latter coincided with the anomalously strong circulation cited above. Over the rest of the 6-year period, significantly northward (southward) displacements of the speed extrema were usually associated with relative minima (maxima) in the regional wind strength indicated by the anomaly mode (Fig. 9). While this accounts for the observed correlations in Table 2, it is not a ubiquitous relationship since some strong anomalies of circulation intensity lack a correspondingly important north-south excursion of the speed extrema (e.g., July 1977, August 1979).

The similarity of the anomaly mode and the southeast trade area index (Table 2, Fig. 9) indicates that interannual southeast trade wind fluctuations behave alike at both the basinwide and SETP regional scales. The strong trades of early 1976, the ensuing weak trades (El Niño) and the final return to strong trades in mid-1977 are clearly reflected at both scales. Note, however, that while the variability is generally similar, important differences may occur, e.g., September–December 1978. Also, the tendency for the SETP region to lead the basin-wide wind field (Table 2) is to some extent discernible in the time series of Fig. 9.

7. Discussion

Consider the 15–30°S latitude range within the SETP region and compare the results of this paper with those of previous studies. In the 15–30°S subregion, nonseasonal fluctuations constitute 50–75% of the total low-level wind-speed variability (Fig. 4a). This nonseasonal variability is highly coherent over the area (Fig. 8a) and has a large interannual component similar to that of the basin-wide SE trades (Fig. 9). Barnett's (1977) EOF analyses of the easterly winds from the Wyrtki-Meyers data set (Pacific-wide, from ship reports) suggested a prominent annual signal over an area extending southeastward to 10–20°S, 85°W, but no conspicuous interannual variability over any part of the SETP region covered by this paper. But from an analysis of autospectra for the 1961–70 tropical Pacific surface winds (also from ship reports), Goldenberg and O'Brien (1981) found the annual signal to be indistinguishable from the background spectrum for the 16–18°S, 84–104°W quadrangle, and the total energy at periodicities of 20 months or more to be relatively high over the subregion in question. The latter analysis is more nearly in agreement with the results of the present study.

The contrasting results of the studies by Barnett (1977) and Goldenberg and O'Brien (1981), which use similar data bases, may be explainable by the fact that Barnett's EOF analysis pooled common variability over the entire tropical Pacific, or ten times the area of the SETP region. Hence, any lack of communality (coherence) between the two scales would cause the noncoherent variability in the smaller area to be isolated by higher EOF modes that appear unimportant on the basin scale. Such a lack of communality may be real, but would also be enhanced by the greater data sparsity (aliasing, noise content) that exists—due to the relative scarcity of ship reports—in the smaller SETP region.

A similar conclusion arises from consideration of the 1972–73 and 1976–77 El Niño episodes. The charts of Ramage *et al.* (1980), based mainly on cloud-vector information in the SETP region, show the winds to have been weaker there during most of the 1972–73 El Niño. This is consistent with a similar finding from this study concerning the 1976–77 event (Figs. 9 and 10). Miller and Laurs (1975) inferred a weakened SETP circulation, during most of 1972, from anomalously low values of a regional SLP index. This is consistent with indications herein (Table 2, Fig. 9) that the surface pressure anomaly for Easter Island is a good proxy index for the nonseasonal SETP circulation strength. But the 700 mb circulation charts of Krueger and Winston (1975), based on NMC objective tropical analyses, show that anomalous *easterly* winds predominated over the 15–30°S portion of the SETP region during 1972. This result is not consistent with Miller and Laurs (1975) nor with the present analysis of the 1976–77 episode. This indicates either that upper air reports are too sparse over the eastern South Pacific to extract meaningful information about the interannual variability there, or that real differences exist between circulation anomalies at 700 mb viz-a-viz lower levels.

Based on 12-hourly surface analyses, Miller and Laurs (1975) concluded that low-pressure weather systems had more equatorward trajectories during the 1972–73 El Niño, disrupting the subtropical high-pressure center and diminishing the trade winds over the SETP region. This is consistent with the unusually high precipitation that is experienced historically at Valparaiso (33°S) in conjunction with El Niño events (Quinn, personal communication) and appears to be the best explanation for the observation that the high-speed core and the anticyclonic center were north of their normal positions during the 1976–77 El Niño (Fig. 9) and statistically so in conjunction with weakened winds (Table 2). The statement by Krueger and Winston (1975) that the South Pacific anticyclone and the SETP trades were displaced south of their normal locations during 1972 is not consistent with these findings.

This study indicates that a simple and effective way to monitor the interannual variability of the SETP circulation is to subtract the long term seasonal mean (Table 1) from the monthly averaged CMV winds at 20°S, 85°W (see Fig. 9). Nonseasonal fluctuations there constitute 60–70% of the total

variability (Fig. 4a) and explain 80% of the areally coherent residual variability (Fig. 8a). Another method, less reliable but simple and supplementary, is to monitor the anomaly of sea level pressure at Easter Island. There appears to be no advantage in subtracting coastal SLP from Easter Island SLP, nor in using upper level pressure heights.

8. Conclusions

This study is primarily an analysis of monthly low-level cloud-motion vector (CMV) winds over the Southeastern Tropical Pacific (SETP) for a 6-year period (1974–80). The most important results of the study are summarized below:

1) The annual cycle of the SETP low-level wind speeds is most prominent north of 15°S, with minimum and maximum intensities during the January–March and July–September periods, respectively, in phase with the basinwide southeast trades.

2) South of 15°S the annual variability is small and characterized by minimum wind speeds from May–July, when the anticyclonic circulation center is at its northernmost position (~26°S).

3) There is an SETP core region of maximum wind speeds that annually migrates (along 85°W) from 20°S in January–March to 15°S in June–August.

4) The SETP circulation is characterized by areally coherent nonseasonal variability over the 15–30°S subregion. When the SETP circulation is unseasonally weak (strong), so is the intensity of the high-speed core, and both the core and the anticyclonic circulation center tend to lie north (south) of their climatological positions.

5) A weak SETP circulation with northward lying positional characteristics prevailed during the 1976–77 El Niño.

6) Peru coastal winds are seasonally in phase with the SE trade circulation at Talara (4°S) and San Juan (15°S) but considerably out of phase at Chimbote (9°S), Lima (12°S) and Tacna (17°S).

7) Nonseasonal variability is poorly correlated or uncorrelated between the coastal winds and various measures of either the basinwide or SETP circulations.

8) Monthly anomalies of the low-level cloud-motion winds at 20°S, 85°W are an effective index of the nonseasonal atmospheric circulation of the SETP region.

Acknowledgments. The author would like to thank Drs. Gary Meyers and James Sadler for their helpful discussions of this work and for generously providing the necessary wind field data. I also wish to thank the Corporacion Peruana de Aviacion Civil (Sr. Guillermo Belevan) and the Armada de Chile (Capt. Jorge Ginouves-Contreras) for providing the fixed station data. The research was supported by National Science Foundation Grants ATM 78-20419 and OCE 80-24116 and by National Oceanic and Atmospheric Administration Contract No. NA80RAC00003.

REFERENCES

Barnett, T. P., 1977: The principal time and space scales of the Pacific trade wind fields. *J. Atmos. Sci.*, **34**, 221–236.

Enfield, D. B., 1981: Thermally driven wind variability in the planetary boundary layer above Lima, Peru. *J. Geophys. Res.*, **86**, 2005–2016.

——, and J. S. Allen, 1980: On the structure and dynamics of monthly sea level anomalies along the Pacific coast of North and South America. *J. Phys. Oceanogr.*, **10**, 557–578.

Goldenberg, S. B. and J. J. O'Brien, 1981: Time and space variability of tropical Pacific wind stress. *Mon. Wea. Rev.*, **109**, 1190–1207.

Gray, W. M., 1972: A diagnostic study of the planetary boundary layer over the oceans. Atmos. Sci. Pap. No. 179, Colorado State University, 95 pp.

Halpern, D., and R. A. Knox, 1981: Coherence between low-level cloud motion vectors and surface easterly tradewind measurements near 0°, 152°W from April 1979–February 1980. Submitted to *J. Geophys. Res.*

Hastenrath, S., and P. J. Lamb, 1977: *Climatic Atlas of the Tropical Atlantic and Eastern Pacific Oceans.* University of Wisconsin Press, Madison.

Hickey, B., 1975: The relationship between fluctuations in sea level, wind stress and sea surface temperature in the equatorial Pacific. *J. Phys. Oceanogr.*, **5**, 460–475.

Hurlburt, H. E., J. C. Kindle and J. J. O'Brien, 1976: A numerical simulation of the onset of El Niño. *J. Phys. Oceanogr.*, **6**, 621–631.

Krueger, A. F. and J. S. Winston, 1975: Large-scale circulation anomalies over the tropics during 1971–72. *Mon. Wea. Rev.*, **103**, 465–473.

McCreary, J., 1976: Eastern tropical ocean response to changing wind systems: with application to El Niño. *J. Phys. Oceanogr.*, **6**, 632–645.

Mendenhall, B. R., 1967: Frictional wind veering in the planetary boundary layer. Atmos. Sci. Pap. No. 116, Colorado State University, 57 pp.

Miller, F. R., and R. M. Laurs, 1975: The El Niño of 1972–73 in the eastern tropical Pacific Ocean. *Int.Amer. Trop. Tuna Comm. Bull.*, **16**, 403–448.

Quinn, W. H., 1974: Monitoring and predicting El Niño invasions. *J. Appl. Meteor.*, **13**, 825–830.

Ramage, C. S., C. W. Adams, A. M. Hori, B. J. Kilonsky and J. C. Sadler, 1980: *Meteorological Atlas of the 1972–73 El Niño.* Rep. No. UHMET 80-03, Dept. of Meteorology, University of Hawaii, 101 pp.

Sadler, J. C., and B. J. Kilonsky, 1981: Trade wind monitoring using satellite observations. Rep. No. UHMET 81-01, Dept. of Meteorology, University of Hawaii.

Sciremammano, F., 1979: A suggestion for the presentation of correlations and their significance levels. *J. Phys. Oceanogr.*, **9**, 1273–1276.

Wyrtki, K., 1975: El Niño—the dynamic response of the equatorial Pacific Ocean to atmospheric forcing. *J. Phys. Oceanogr.*, **5**, 572–584.

——, 1979: The response of sea surface topography to the 1976 El Niño. *J. Phys. Oceanogr.*, **9**, 1223–1231.

——, and G. Meyers, 1976: The trade wind field over the Pacific Ocean. *J. Appl. Meteor.*, **15**, 698–704.